

The effect of a fissure on storage in a porous medium

JEROME A. NEUFELD†, DOMINIC VELLA
AND HERBERT E. HUPPERT

Institute of Theoretical Geophysics, Department of Applied Mathematics and Theoretical Physics,
University of Cambridge, Wilberforce Road, Cambridge CB3 0WA, UK

(Received 7 May 2009; revised 29 June 2009; accepted 30 June 2009; first published online
12 October 2009)

We consider the two-dimensional buoyancy driven flow of a fluid injected into a saturated semi-infinite porous medium bounded by a horizontal barrier in which a single line sink, representing a fissure some distance from the point of injection, allows leakage of buoyant fluid. Our studies are motivated by the geological sequestration of carbon dioxide (CO₂) and the possibility that fissures in the cap rock may compromise the safe long-term storage of CO₂. A theoretical model is presented that accounts for leakage through the fissure using two parameters, which characterize leakage driven both by the hydrostatic pressure within the overriding fluid and by the buoyancy of the fluid within the fissure. We determine numerical solutions for the evolution of both the gravity current within the porous medium and the volume of fluid that has escaped through the fissure as a function of time. A quantity of considerable practical interest is the efficiency of storage, which we define as the amount of fluid remaining in the porous medium relative to the amount injected. This efficiency scales like $t^{-1/2}$ at late times, indicating that the efficiency of storage ultimately tends to zero. We confirm the results of our model by comparison with an analogue laboratory experiment and discuss the implications of our two-dimensional model of leakage from a fissure for the geological sequestration of CO₂.

1. Introduction

Buoyancy driven flow of fluid through a layered porous medium occurs throughout many environmental and industrial settings. Important examples include groundwater flows and the contamination of aquifers, the motion of oil and natural gas in petroleum reservoirs and the characterization of geothermal systems (see for example Bear 1972; Phillips 2009). More recently, concern for the long-term fate of the Earth's climate has galvanized efforts to mitigate anthropogenic climate change. Approximately 27 gigatonnes of carbon dioxide (CO₂) are released annually by mankind into the atmosphere, likely leading to a precipitous rise in the average global temperature. One of the most promising methods for combating this dangerous increase is through carbon capture and storage (CCS). This process, in which large quantities of CO₂ are captured and then stored within geological reservoirs, has generated much recent interest in buoyancy driven flows in layered geological strata (Nordbotten, Celia & Bachu 2005a; Vella & Huppert 2006; Bickle *et al.* 2007; Neufeld & Huppert 2009). However, to be truly effective, storage requires relatively permeable formations in

† Email address for correspondence: j.neufeld@damtp.cam.ac.uk

which to inject the CO₂, without compromising the stability of the sequestered CO₂ on 1000 year time scales. This latter requirement motivates the present investigation of the efficiency of storage in reservoirs punctuated by fissures or faults.

The study of buoyancy driven flows, or gravity currents, within layered permeable rock is well developed, including both flows in unconfined reservoirs (Barenblatt 1996; Anderson, McLaughlin & Miller 2003; Lyle *et al.* 2005) and confined geometries (Huppert & Woods 1995). Several studies, such as those reviewed in Huppert (2006), have shown that in many situations the horizontal scale of the buoyancy driven flow greatly exceeds the vertical scale and therefore pressure is approximately hydrostatic in the vertical. In horizontal strata, it is the lateral gradients in the depth of the fluid that drive flow, a simplification that leads to a nonlinear evolution equation describing the sharp interface between buoyant and ambient reservoir fluids. When such reservoirs are bounded by one or more impermeable barriers this evolution equation generally admits similarity solutions which are a powerful tool with which to quickly assess the characteristics of subsurface flows. For example, Bickle *et al.* (2007) recently used a robust seismic estimate of the extent of a CO₂ plume injected beneath the North Sea along with the scaling laws developed by Lyle *et al.* (2005) to infer reservoir properties as a function of depth within the formation.

These depth-integrated models have been extended to include the effects of both diffuse and discrete leakage through the boundaries. Pritchard, Woods & Hogg (2001) modelled the propagation of fluid over, and distributed drainage through, a relatively thin lower permeability layer. They considered the limit where drainage is driven solely by the hydrostatic pressure of the overriding fluid in both two-dimensional and axisymmetric geometries. Acton, Huppert & Worster (2001) examined the related problem of a two-dimensional viscous gravity current propagating over a deep porous medium both experimentally and numerically. They considered drainage driven by both the hydrostatic pressure of the viscous fluid, as well as the weight of fluid within the underlying porous medium. Following this work, Pritchard & Hogg (2002) considered the related problem of flow in a layered two-dimensional porous medium using an identical drainage law. In the axisymmetric geometry, Spanuth *et al.* (2009) observed experimentally that viscous currents spreading radially over an ideal porous media are well characterized using the drainage law proposed by Acton *et al.* (2001). Such diffuse drainage laws have been used by Neufeld & Huppert (2009) to model the propagation of injected CO₂ through the layered Utsira formation beneath the North Sea. Finally, Farcas & Woods (2009) and Woods & Farcas (2009) have proposed a model for capillary retention in layered formations, in which a critical fluid depth must be exceeded before diffuse drainage can begin. They have applied this model to both horizontal and sloping two-dimensional formations.

Models examining the effect of discrete leakage points through the boundary have been motivated recently by the geological storage of contaminants or CO₂. These studies have chiefly examined the effect of the pressure field accompanying injection. Nordbotten, Celia & Bachu (2004) and Nordbotten *et al.* (2005*b*) built on the work of Avci (1994) who modelled leakage driven solely by the increased pressure associated with injection into a confined aquifer. More recently, Nordbotten *et al.* (2009) have proposed a method for incorporating the effect of buoyancy on leakage in a confined aquifer. Finally, Pritchard (2007) has studied the buoyancy driven propagation of a gravity current in a two-dimensional porous medium with a series of line sinks or fissures spaced symmetrically about the injection point. That study provided both numerical solutions of the full time-dependant problem, as well as an asymptotic analysis of the long-term behaviour. Importantly, Pritchard (2007) found that the

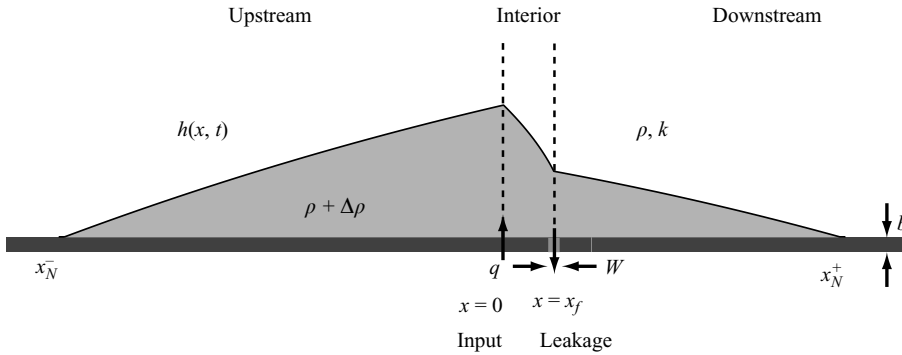


FIGURE 1. A current of density $\rho + \Delta\rho$ is input at constant rate at the origin. It spreads into a porous medium of permeability k saturated with an ambient fluid of density ρ . At a distance x_f from the origin the current spreads over a fissure of permeability k_f , through which it drains, producing a marked difference in the length of the current to the right $x_N^+(t)$ and left $x_N^-(t)$ as functions of time.

profile of the current quickly reaches a steady state governed principally by a non-dimensional measure of the strength of the line sink.

In the present work we expand the model of Pritchard (2007) to consider the propagation of a two-dimensional gravity current within a porous medium with an asymmetric geometry more typical of geological reservoirs. We consider the effect of a single line sink or fissure some distance from the injection point. A model of drainage through the fissure is formulated in § 2, which incorporates both flow driven by hydrostatic pressure as well as the weight of the fluid within the fissure itself, which was neglected by Pritchard (2007). This model is coupled to the standard equations governing flow of a thin buoyant fluid within a porous medium. In § 3 we show that the system approaches a steady state and we compare numerical computations and asymptotic expressions for the efficiency of storage. These models are then tested against the results of an analogue Hele-Shaw cell experiment in § 4. In § 5 we consider the relevance of our predictions for the geological sequestration of CO_2 and the storage of contaminants. We conclude with some possibilities for future research and a discussion in § 6.

2. Theoretical development

2.1. Geometry

Consider injection, at constant volume flux q , of a fluid of density $\rho + \Delta\rho$ flowing into a semi-infinite porous medium of permeability k saturated with fluid of density ρ as depicted in figure 1. The semi-infinite medium is bounded by an impermeable horizontal barrier through which a fissure of width W and permeability k_f allows leakage of the injected fluid centred at a distance x_f from the injection point. For clarity, we term the current between the source and the fissure the ‘interior current’. Fluid which flows past the fissure forms the ‘downstream current’ while that which leaves the source moving away from the fissure forms the ‘upstream current’ as depicted in figure 1. The sharp interface between injected and ambient fluids is described by the thickness $h(x, t)$, which evolves with time t and is a function of the distance from the injection point x . We note that when the depth of the reservoir greatly exceeds the typical thickness of the current the pressure associated with

injection is negligible and the flow is driven principally by the density difference. Such gravity currents typically have much greater horizontal than vertical extent. Flow within the current is predominantly horizontal and therefore the pressure is effectively hydrostatic. Crucially, we note that the quantitative behaviour of such currents is identical for the case of a dense fluid released above a leaky barrier (as shown in figure 1 and in the experiments of §4) or for a buoyant fluid released below a cap rock, as is the case for the geological sequestration of CO₂. Finally, for simplicity we consider only the case where the two fluids have equal viscosity ν , although we note that for CO₂ sequestration the kinematic viscosity of the brine is 10–20 times that of the CO₂ at representative reservoir temperatures and pressures (Bachu & Bennion 2008). This viscosity contrast would likely lead to a more diffuse interface which we neglect to simplify our analysis.

2.2. Drainage and propagation

We consider a general form of drainage through the fissure motivated by both the variety of geological reservoirs, and by the experiments of §4 which show clearly that drainage through the fissure is driven both by the hydrostatic pressure within the current and by the weight of the fluid within the fissure itself. We use the form of drainage proposed by Acton *et al.* (2001) and used successfully to model the drainage of a viscous current over a porous bed in two-dimensions (Acton *et al.* 2001), in three dimensions (Spannuth *et al.* 2009) and within layered porous media (Pritchard & Hogg 2002; Neufeld & Huppert 2009). For a fissure of width $W \ll x_f$ and permeability k_f , spanning the depth b of an impermeable layer the Darcy velocity within the fissure is primarily vertical, and given by

$$v_f(x, t) = -\frac{k_f \Delta\rho g(h+b)}{\mu b} = -\phi\gamma \frac{k_f}{k} \left[1 + \frac{h(x, t)}{b} \right], \quad |x - x_f| < W/2, \quad (2.1)$$

where $\gamma \equiv k\Delta\rho g/\phi\mu$ is the characteristic velocity within the reservoir, ϕ is the porosity of the matrix which, for simplicity, is assumed equal between the reservoir and the fissure and g is the local acceleration due to gravity. We assume that the depth of the fissure b is at least the same order as $h(x_f, t)$. The evolution of the height of the buoyant current is therefore governed by

$$\frac{\partial h}{\partial t} - \gamma \frac{\partial}{\partial x} \left(h \frac{\partial h}{\partial x} \right) = -\gamma \frac{k_f}{k} \left(1 + \frac{h}{b} \right) \mathcal{F}(x, x_f, W), \quad (2.2)$$

where

$$\mathcal{F}(x, A, B) \equiv \begin{cases} 0 & |x - A| > B/2 \\ 1 & |x - A| < B/2 \end{cases}$$

is a Boxcar centred on A , with width B and unit magnitude and which mathematically describes the localized nature of drainage through the fissure. To (2.2) we add three boundary conditions,

$$\left[\gamma h \frac{\partial h}{\partial x} \right]_{x=0^-}^{x=0^+} = -q, \quad \left[\gamma h \frac{\partial h}{\partial x} \right]_{x=x_N^+} = 0, \quad (2.3a, b, c)$$

which describe the constant flux input at the origin and the requirement that there be zero flux through the two noses of the current, respectively. Here x_N^+ and x_N^- denote the distance from the source to the nose of the downstream and upstream currents respectively, as depicted in figure 1.

2.3. Non-dimensionalization

The propagation of a gravity current past a fissure or line sink, defined by (2.2) with boundary conditions (2.3a–c), can be made non-dimensional in the following manner. We note that the presence of the fissure introduces a natural horizontal length scale X , such that the problem is readily scaled by

$$X \equiv x_f, \quad H \equiv (x_f q / \gamma)^{1/2} \quad \text{and} \quad T \equiv (x_f^3 / q \gamma)^{1/2}, \quad (2.4a, b, c)$$

where H is the vertical length scale and T the time scale. It is clear from the form of the drainage law that the fissure can now be characterized by three parameters. The strength of the fissure is characterized by

$$\lambda \equiv \frac{k_f}{k} \frac{1}{b} (x_f^3 \gamma / q)^{1/2}, \quad (2.5)$$

while the vertical extent and width of the fissure are given by

$$\beta \equiv b(\gamma / x_f q)^{1/2} \quad \text{and} \quad \epsilon \equiv W / x_f, \quad (2.6a, b)$$

respectively. Equations (2.2)–(2.3) are non-dimensionalized using the scales (2.4a–c) and become

$$\frac{\partial h}{\partial t} - \frac{\partial}{\partial x} \left(h \frac{\partial h}{\partial x} \right) = -\lambda(\beta + h) \mathcal{F}(x, 1, \epsilon), \quad (2.7)$$

$$\left[h \frac{\partial h}{\partial x} \right]_{x=0^-}^{x=0^+} = -1, \quad \left[h \frac{\partial h}{\partial x} \right]_{x=x_N^\pm} = 0. \quad (2.8a, b, c)$$

Finally, we note that the form of drainage given by (2.1) is similar to that used by Pritchard (2007) when the height of the current above the fissure is much greater than its vertical extent $h(1) \gg \beta$. We shall see in §3 that in the long time limit $h(1) \sim 1/(\epsilon \lambda)$. Therefore, $h(1) \gg \beta$ corresponds to the dimensional limit of a narrow fissure defined by

$$W \ll \frac{k}{k_f} \frac{q}{\gamma}. \quad (2.9)$$

A direct comparison of (2.7) can be made with the analysis of Pritchard (2007) by integrating the drainage across the width of the sink,

$$0 = \int_{1-\epsilon/2}^{1+\epsilon/2} \frac{\partial h}{\partial t} dx = \left[h \frac{\partial h}{\partial x} \right]_{1-\epsilon/2}^{1+\epsilon/2} - \epsilon \lambda(\beta + \bar{h}), \quad (2.10)$$

where

$$\bar{h} \equiv \frac{1}{\epsilon} \int_{1-\epsilon/2}^{1+\epsilon/2} h dx \quad (2.11)$$

is the average height above the fissure. We therefore see that the width-averaged leakage flux is given by $\bar{\lambda}(\beta + \bar{h})$ where

$$\bar{\lambda} \equiv \epsilon \lambda = \frac{k_f}{k} \frac{W}{b} (x_f \gamma / q)^{1/2}. \quad (2.12)$$

This parameter $\bar{\lambda}$ is precisely that derived by Pritchard (2007) for leakage from fissures placed symmetrically about an injection well.

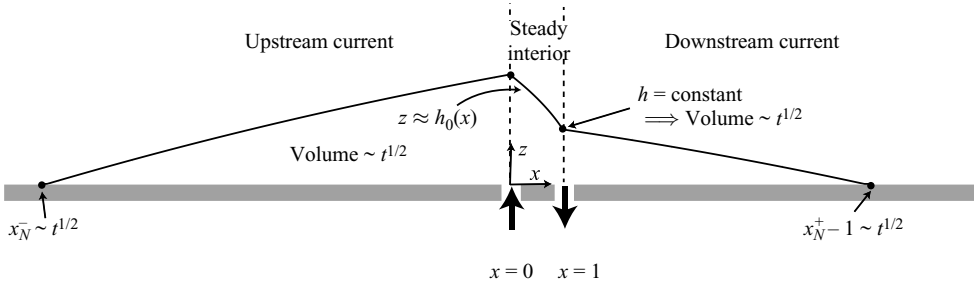


FIGURE 2. Schematic diagram showing the three regions observed at long times. The current approaches a steady shape in $0 < x < 1$. The heights at $x = 0$ and $x = 1$ are therefore constant so that trapped currents form in the regions $x < 0$ and $x > 1$. Such currents must have a volume $\sim t^{1/2}$ and an extent $\sim t^{1/2}$, as indicated by extending a calculation of Huppert & Woods (1995).

3. The approach to steady-state leakage

We follow the approach of Pritchard (2007) who noted that the leakage from the current, being driven to a large extent by the height of the fluid above the fissure, always tends to a steady state in which the flux of fluid injected into the reservoir is matched by that leaking out through the fissure. This unexpected final state can be anticipated by noting that, for currents fed by a constant flux, the height increases over time leading to a concomitant increase in leakage. We note that in the steady state the height above the injection point, as well as that above the fissure, are constant. To sustain such steady heights, the analysis by Huppert & Woods (1995) shows that the volumes which flow into the regions $x < 0$ and $x > 1$ must both scale like $t^{1/2}$. For this reason the horizontal extent of the trapped currents must also grow like $t^{1/2}$. A schematic picture of this scenario is shown in figure 2. Here we begin by considering analytically this scenario. In what follows we confirm this picture with numerical solutions to the full problem described by (2.7)–(2.8) which compare very favourably with our analytical solutions for the asymptotic state.

3.1. The interior current ($0 < x < 1$)

In the region $0 < x < 1$ we look for a solution of the form $h(x, t) = h_0(x) + t^{-1/2} h_1(x) + O(t^{-1})$. Substituting this form into (2.7), we find that, at leading order in time,

$$h_0^2 = A_0 + B_0 x, \tag{3.1}$$

for constants A_0 and B_0 . Applying the flux condition at the origin (2.8a), we find that $B_0 = -2$. Since the leakage flux equals the input flux in the final steady state we can determine that $\bar{\lambda}[\beta + h_0(1)] = 1$. The profile between the source and fissure is therefore given by

$$h_0(x) = [2 + (\bar{\lambda}^{-1} - \beta)^2 - 2x]^{1/2}, \tag{3.2}$$

which recovers the steady-state profile presented by Pritchard (2007) in the limit $\beta \rightarrow 0$. To calculate the asymptotic behaviour of the leakage fluxes in the other regions it is also necessary to calculate the next order term, which satisfies

$$h_0 h_1 = A_1 + B_1 x. \tag{3.3}$$

The constant B_1 will be determined by conserving flux at the origin and therefore requires the calculation of the flow in the region $x < 0$.

3.2. The upstream current ($x < 0$)

To leading order in time, the height above the injection point is constant. The current in the region $x_N^- < x < 0$ will therefore have a flux proportional to $t^{-1/2}$ (see Huppert & Woods 1995, §3). Furthermore, the natural similarity variable in this region is $\zeta \equiv -x/t^{1/2}$ and we therefore pose a series solution of the form

$$h(x, t) = H_0^-(\zeta) + t^{-1/2}H_1^-(\zeta) + O(t^{-1}). \tag{3.4}$$

At leading order in time (2.7) then gives

$$-\zeta \frac{dH_0^-}{d\zeta} = \frac{d^2H_0^-}{d\zeta^2}. \tag{3.5}$$

The boundary conditions governing solutions to (3.5) at leading order are found as follows. From the form of the two-dimensional similarity solution, where volume increases as $t^{1/2}$, we anticipate that the nose of the current is given by $x_N^- \propto t^{1/2}$. Therefore, in the similarity coordinates, the position of the nose is given by $\zeta = \zeta_0$, a constant. Thus, writing the constraint $h(x_N^-, t) = 0$ and using the similarity variable, we find that

$$H_0^-(\zeta_0) = 0. \tag{3.6}$$

The kinematic condition,

$$\frac{dx_N^-}{dt} = -\left. \frac{\partial h}{\partial x} \right|_{x_N^-}, \tag{3.7}$$

becomes

$$-\frac{\zeta_0}{2} = \left. \frac{dH_0^-}{d\zeta} \right|_{\zeta_0}. \tag{3.8}$$

Finally, at the origin the height of the current equals the steady-state solution (3.2) for $0 < x < 1$, and therefore

$$H_0^-(0) = h_0(0) = [2 + (\bar{\lambda}^{-1} - \beta)^2]^{1/2}. \tag{3.9}$$

The system composed of (3.5) together with boundary conditions (3.6) and (3.8) can be solved by introducing the scaled variable

$$\chi \equiv 1 - \zeta/\zeta_0, \tag{3.10}$$

and letting

$$\varphi(\chi) \equiv H_0^-/\zeta_0^2. \tag{3.11}$$

Equation (3.5) then becomes

$$\frac{d^2\varphi^2}{d\chi^2} = (1 - \chi) \frac{d\varphi}{d\chi}. \tag{3.12}$$

Solutions to (3.12) are to be found subject to the boundary conditions

$$\varphi(0) = 0, \quad \varphi'(0) = 1/2, \tag{3.13a, b}$$

which are the rescaled versions of boundary conditions (3.6) and (3.8). The numerical solution of (3.12) subject to (3.13a–b) provides a value of the height of the upstream current at the origin, and therefore determines ζ_0 through boundary condition (3.9),

$$\zeta_0 = \frac{[2 + (\bar{\lambda}^{-1} - \beta)^2]^{1/4}}{\varphi(1)^{1/2}}. \tag{3.14}$$

We may now determine the value of B_1 . Balancing the fluxes at the origin, we write

$$-1 = \left[h \frac{\partial h}{\partial x} \right]_{x=0^-}^{x=0^+} = \frac{B_0}{2} + B_1 t^{-1/2} + t^{-1/2} H_0^- \left. \frac{dH_0^-}{d\xi} \right|_{\xi=0} + O(t^{-1}), \tag{3.15}$$

and find that at $O(t^{-1/2})$

$$B_1 = -H_0^-(0) \left. \frac{dH_0^-}{d\xi} \right|_{\xi=0} = \zeta_0^3 \varphi(1) \varphi'(1). \tag{3.16}$$

From numerical integration of (3.12) we find that $\varphi(1) = 0.383$ and $\varphi'(1) = 0.275$. This completes the description of the upstream extent of the current and the magnitude of the flux towards the fissure (through the specification of B_1) to leading order.

3.3. The downstream current ($x > 1$)

We now turn our attention to the region beyond the fissure $1 < x < x_N^+$. The analysis here is much the same as in the case of the upstream current and so we present only a brief outline of the solution. For $x > 1$ we define the natural similarity variable $\xi \equiv (x - 1)/t^{1/2}$ and expand $h(x, t)$ as

$$h(x, t) = H_0^+(\xi) + t^{-1/2} H_1^+(\xi) + O(t^{-1}).$$

Our choice of similarity variable recovers the form of the ordinary differential equation governing the height of the upstream current,

$$-\xi \frac{dH_0^+}{d\xi} = \frac{d^2 H_0^{+2}}{d\xi^2}, \tag{3.17}$$

along with boundary conditions

$$H_0^+(\xi_0) = 0, \quad \left. \frac{dH_0^+}{d\xi} \right|_{\xi_0} = 0. \tag{3.18a, b}$$

Repeating the rescalings in (3.10) and (3.11) we recover the system (3.12)–(3.13), the solution of which now provides the height of the downstream current at the fissure. This therefore determines the constant ξ_0 , given by

$$\xi_0 = \left[\frac{\bar{\lambda}^{-1} - \beta}{\varphi(1)} \right]^{1/2}. \tag{3.19}$$

3.4. The leakage flux

While the quantities in (3.14) and (3.19) allow us to track the progress of both the upstream and downstream currents as a function of parameters $\bar{\lambda}$ and β , a more practically relevant quantity is the flux that leaks out of the reservoir through the fissure. The evolution of the leakage flux can now be evaluated, to leading order, as the difference between the flux of fluid injected into the reservoir and the fluxes of fluid into the upstream and downstream currents. We first note that the leakage flux is simply given by the jump in flux between the interior current ($0 < x < 1$) and the downstream current ($x > 1$):

$$\begin{aligned} q_f(1, t) &= \left[h \frac{\partial h}{\partial x} \right]_{x=1^-}^{x=1^+} = t^{-1/2} H_0^+(0) \left. \frac{dH_0^+}{d\xi} \right|_{\xi=0} - \left[\frac{B_0}{2} + t^{-1/2} B_1 \right] + O(t^{-1}) \\ &= 1 - t^{-1/2} \varphi(1) \varphi'(1) [\xi_0^3 + \zeta_0^3] + O(t^{-1}). \end{aligned} \tag{3.20}$$

Perhaps more pertinently, by integrating this flux over the lifetime of injection into the reservoir we can estimate a long-term efficiency of storage, defined by

$$E_s \equiv \frac{V_{\text{current}}}{V_{\text{injected}}}. \quad (3.21)$$

Thus,

$$\begin{aligned} E_s &= 1 - \frac{1}{t} \int_0^t q_f(1, t') dt' \\ &= 2\varphi(1)\varphi'(1)[\xi_0^3 + \zeta_0^3] t^{-1/2} + O(t^{-1}), \end{aligned} \quad (3.22)$$

which shows that in the long-term limit the efficiency of storage decays to zero as $t^{-1/2}$.

3.5. Approach to the asymptotic state

The full time-dependent behaviour of the trapped currents defined by (2.7)–(2.8) has been calculated numerically using the method detailed in Appendix A. For each simulation the currents are initiated with zero height everywhere. At time $t=0$ fluid is introduced at the origin and initially the current follows the similarity solution described by Huppert & Woods (1995) until the current reaches the fissure at $x=1$.

Numerically, drainage at the fissure is implemented using a non-dimensional analogue of (2.1) given by

$$v_f = \lambda[\beta(1 - e^{-\delta h}) + h(1)], \quad (3.23)$$

where we have chosen $\delta = 25 \gg W/h$ to preserve the physical limit $v_f \rightarrow 0$ as $h \rightarrow 0$ and note that this choice does not affect the behaviour of the solutions once $h(1) \gg \delta^{-1}$. Numerically, the fissure width ϵ is taken to be the grid spacing Δx at time $t=0$ so that $\bar{\lambda} = \Delta x \lambda$.

The evolution of both the currents and the leakage flux depends greatly on the width-averaged strength of the fissure $\bar{\lambda}$ as shown in figure 3 for $\beta=0$. We find that for $\bar{\lambda}=0$ the similarity solution is recovered. As $\bar{\lambda}$ is then increased the asymmetry in the lateral extents of the current also increases. This is seen most dramatically in figure 4 where we plot the ratio of the extents x_N^+/x_N^- as a function of t for various $\bar{\lambda}$, again for $\beta=0$. Most importantly, the efficiency of storage defined as the ratio between the volume retained in the current and the volume of fluid injected (3.21), can be calculated. Figure 5 shows the numerical calculations of reservoir efficiency as a function of $\bar{\lambda}$ for $\beta=0$ (solid curves) along with the asymptotic predictions of (3.22) (dashed lines). We see that for small values of $\bar{\lambda}$ the numerical solutions converge relatively slowly to the asymptotic expressions given by (3.22), while for large $\bar{\lambda}$ the approach is quite fast. Finally, in figure 6 we show the comparison between numerical and asymptotic values of E_s for $\bar{\lambda}=1$ and two values of β . We find that as the non-dimensional vertical extent of the fissure β is increased, the efficiency of storage is decreased. This is because fluid escapes the reservoir far more quickly when the fissure is deeper (β greater), thus enabling the buoyant fluid within the fissure to exert a stronger pull on fluid within the reservoir. In our analysis of the late-time behaviour this is reflected in an increase in the effective value of $\bar{\lambda}$ when $\beta > 0$.

4. Experimental analogue

A series of five experiments were performed in a Hele-Shaw cell as a test of the numerical and asymptotic analysis of the two-dimensional source-sink problem.

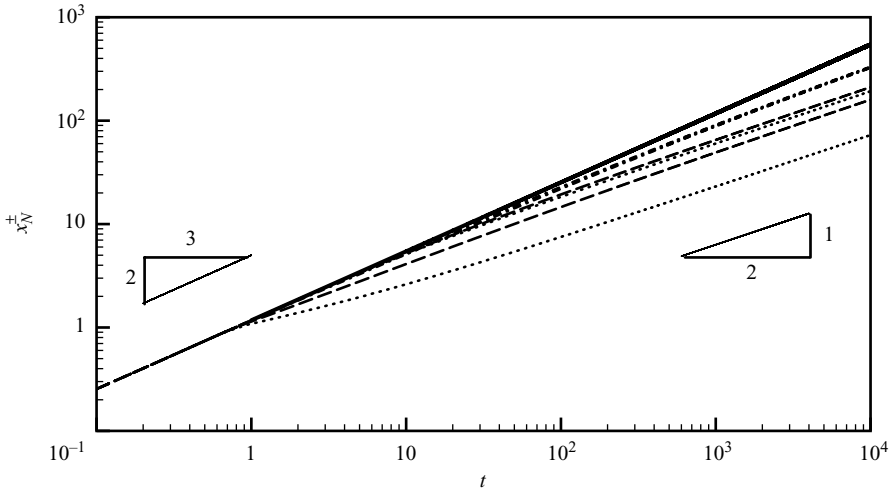


FIGURE 3. A measure of the asymmetry of the resultant currents. We plot the extent of the upstream (x_N^-) and downstream (x_N^+) currents as a function of time for varying strengths of the fissure $\bar{\lambda}$ in the limit in which buoyancy is negligible within the fissure ($\beta \rightarrow 0$). In each case, the downstream current propagates farther than the upstream current, i.e. $x_N^+ < x_N^-$, with the difference becoming more dramatic as $\bar{\lambda}$ is increased. When the fissure strength is reduced to zero, $\bar{\lambda} = 0$, and before any current has reached the fissure, the classic similarity solution ($x_N^\pm \sim t^{2/3}$, bold solid) is recovered. For $\bar{\lambda} = 0.2$ (dash-dot), $\bar{\lambda} = 1$ (dashed) and $\bar{\lambda} = 5$ (dotted) the influence of drainage through the fissure becomes increasingly important. Note that the currents initially propagate as $t^{2/3}$ before subsequently relaxing to the long-time asymptotics $\sim t^{1/2}$.

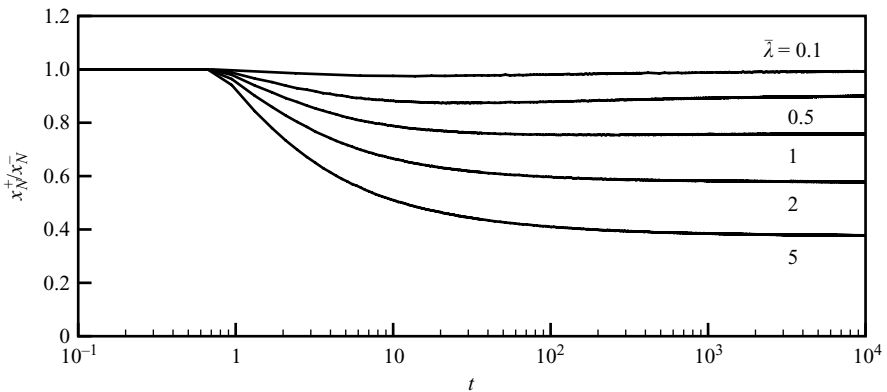


FIGURE 4. Ratio of the downstream (x_N^+) to upstream (x_N^-) extents of the current for $\beta = 0$, and a variety of $\bar{\lambda}$.

These experiments directly test the validity of both the functional form of the drainage velocity and its inclusion within the lubrication approximation as a flux jump across the fissure.

The experimental apparatus consisted of a vertical Hele-Shaw cell of cross-sectional width $d = 0.48$ cm, length 196.4 cm and height 30 cm as depicted in figure 7. Fluid was injected at the centre of the cell ($x = 0$ cm) using a Watson Marlow 505U peristaltic pump from a reservoir whose mass was recorded as a function of time

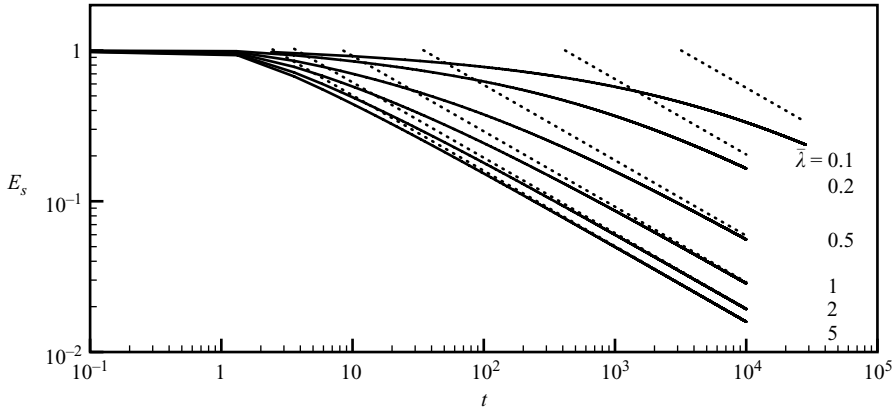


FIGURE 5. Efficiency of storage E_s defined in (3.21) for $\beta = 0$ and a variety of $\bar{\lambda}$. Full numerical solutions of (2.7) are shown as solid curves and the asymptotic solutions (3.22) are shown by the dotted lines.

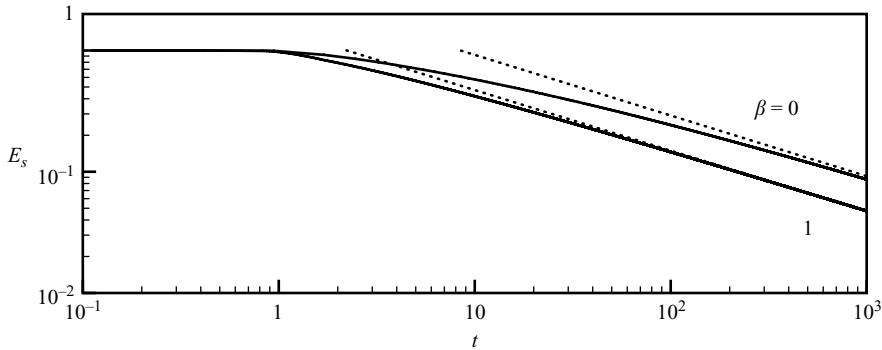


FIGURE 6. Efficiency of storage E_s for $\bar{\lambda} = 1$ with $\beta = 0$ and $\beta = 1$. Full numerical solutions of (2.7) are shown as solid curves and the asymptotic solutions (3.22) are shown by the dotted lines.

using a digital mass balance. This provided a precise measure of the constant flux of fluid injected during each experiment. A total of five experiments were conducted, as reported in table 1. For each experiment the viscosity and input flux were measured independently.

The fissure consisted of a gap of width $W = 1.1$ cm and vertical extent $b = 2.1$ cm in the base of the Hele-Shaw cell located a distance $x_f = 11$ cm from the injection point. The mass of fluid which drained from the sink was also recorded digitally as a function of time and compared with the results of §3. The extent of the current both in the direction towards the sink (x_N^+) and away from the sink (x_N^-) was recorded at 5 s intervals. The profile of a typical current is shown in figure 8. Initially, fluid spread symmetrically about the injection point following the similarity solution outlined by Huppert & Woods (1995). As shown by the photograph of a representative experiment in figure 8, once the current reached the fissure a definite asymmetry developed between the upstream and downstream currents. This was accompanied by a jump in the slope of the free surface associated with the leakage flux through the base of the tank.

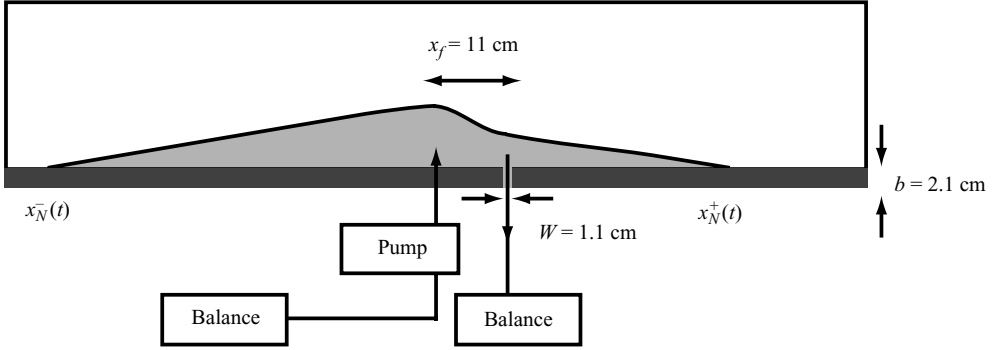


FIGURE 7. Geometry of the analogue Hele-Shaw cell experiments. Input and leakage fluxes were measured with digital mass balances and the profiles recorded with a digital camera.

Experiment	q (cm ² s ⁻¹)	ν (cm ² s ⁻¹)	H (cm)	T (s)	$\bar{\lambda}$	β	Symbol
1	4.066 ± 0.004	7.85 ± 0.08	4.32	11.68	0.626	0.486	◇
2	6.995 ± 0.005	7.4 ± 0.2	5.50	8.65	0.491	0.382	▽
3	5.90 ± 0.01	5.9 ± 0.1	4.51	8.41	0.599	0.466	□
4	5.021 ± 0.003	7.0 ± 0.1	4.53	9.93	0.596	0.464	○
5	6.914 ± 0.007	6.4 ± 0.1	5.08	8.09	0.531	0.413	△

TABLE 1. A total of five experiments were conducted in which the flux q and viscosity ν were varied. The corresponding vertical scale H and temporal scale T along with the non-dimensional parameters $\bar{\lambda}$ and β are given, as defined by (2.4b-c), (2.12) and (2.6a), respectively. These parameters are estimated using the global fit of drainage data to constrain $k_f = 9 \times 10^{-3}$ cm².

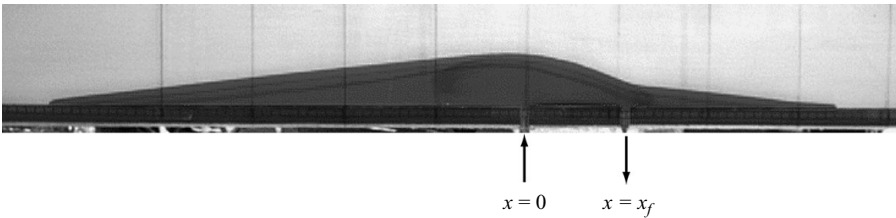


FIGURE 8. Profile of a viscous current within a Hele-Shaw cell with a fissure located a distance $x_f = 11$ cm from the source.

Experiments, typified by the image in figure 8, were analysed in the following manner. First, the validity of the drainage law given by (2.1) was assessed, and the permeability of the fissure quantified, by correlating the measured output flux to the height above the fissure. Digital images of the current above the sink (taken every two seconds) were processed in Matlab to provide an automated estimate of the height above the sink, $h(x_f)$. Simultaneously, the digital mass balance recorded the mass of fluid leaving the sink, from which a drainage velocity v_f was calculated. The results of five experiments were fitted to a drainage velocity of the form used in (3.23),

$$v_f = -\gamma \frac{k_f}{k} \left[1 - \exp(-5h/W) + \frac{h}{b} \right], \quad (4.1)$$

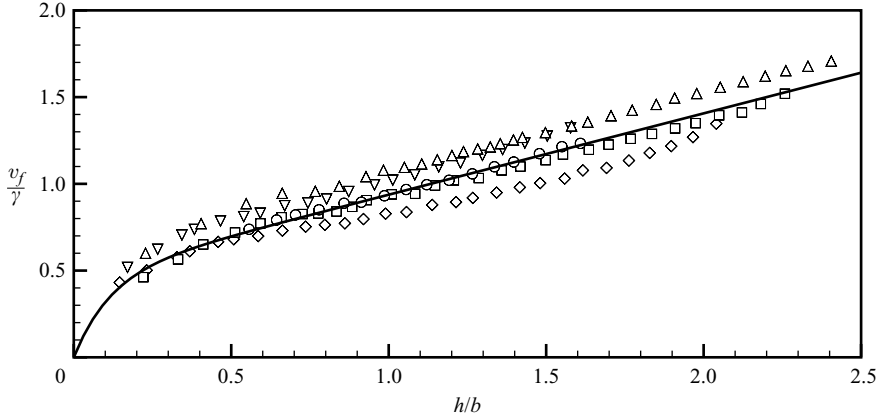


FIGURE 9. Experimental measurements and the corresponding fit of the theoretical model for the non-dimensional drainage velocity through the fissure as a function of the observed height above the fissure. Experimental data (symbols) are for the five experiments as described in table 1. The drainage model (4.1) is fit to the experimental data using a globally fitted fissure permeability, $k_f = 9 \times 10^{-3} \text{ cm}^2$.

as shown in figure 9. This provided a universal measure of the permeability of the fissure of

$$k_f = 9 \times 10^{-3} \text{ cm}^2. \quad (4.2)$$

This value can be compared with the theoretical estimate given by Happel & Brenner (1991) for a rectangular channel of cross-section $d \times W$ which is

$$\begin{aligned} k_f &= d^2 + W^2 \\ &\quad - \frac{8}{\pi^5 d W} \sum_{n=1}^{\infty} \frac{1}{(2n-1)^5} \left[d^4 \tanh\left(\frac{2n-1}{2} \frac{\pi W}{d}\right) + W^4 \tanh\left(\frac{2n-1}{2} \frac{\pi d}{W}\right) \right] \\ &= 13.9 \times 10^{-3} \text{ cm}^2. \end{aligned} \quad (4.3)$$

The discrepancy in these values is likely due to one of four factors. Flow within the rectangular fissure may not fully realize the description of Happel & Brenner (1991) within its length b ; irregularities in the rectangular channel may decrease the effective permeability; pressure at the outlet may not be strictly the ambient (a central assumption of our drainage model); and finally, the three-dimensional flow structure around the fissure may reduce the effective permeability. The values of $\bar{\lambda}$ and β derived from the system parameters and the universal fit for k_f (given in (4.2)) for each experimental run are given in table 1.

Our estimates of the parameters presented in table 1 enable us to predict the profile of the current for each experimental realization. A comparison is made between the measured extents of both upstream (x_N^-) and downstream (x_N^+) currents in figure 10. Here care must be taken to account for flow within the Hele-Shaw cell. As detailed in Appendix B, when $h \gg d$, the width-averaged equations governing flow within the Hele-Shaw cell provide an exact analogue to dispersionless flow within a porous media with a permeability given by

$$k = \frac{d^2}{12}. \quad (4.4)$$

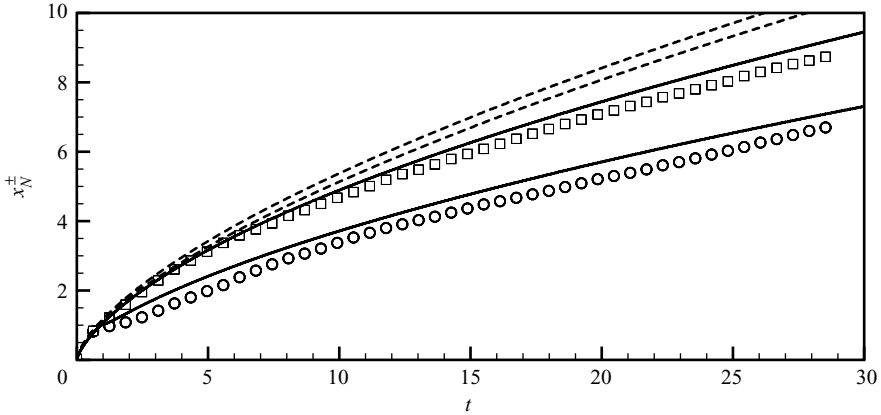


FIGURE 10. Representative comparison between the experimental extents of the current and the theoretical predictions, here for experiment 5 (see table 1 for parameters). The experimentally measured upstream extent (x_N^- , squares) and downstream extent (x_N^+ , circles) are shown along with the numerical predictions both including the effects of bottom friction (solid) and neglecting the effects of the bottom boundary of the Hele-Shaw cell (dashed). The effect of bottom friction was incorporated using an effective permeability, $k_{eff}(h)$, with dimensionless cell width $d/H = 0.094$ (see Appendix B for details).

However, when the thickness of the current is comparable to the width of the tank, $h \sim d$, the effect of friction at the base of the Hele-Shaw cell can become significant. This effect is particularly striking in our asymmetric gravity currents since the upstream current is typically much thicker than the downstream current that propagates past the fissure. We therefore use an effective permeability k_{eff} , whose derivation is detailed in Appendix B. This effective permeability is now a function of the ratio of current height to the cross-sectional width of the tank, $k_{eff} = k_{eff}(h/d)$, and it provides a much more satisfactory account of the extent of the spreading current. The difference in predictive power is striking. In figure 10 the numerical predictions including the added effect of bottom friction in the Hele-Shaw cell are shown by the solid curves, while those neglecting bottom friction are shown by the dashed curves. Clearly much of the reduction in extent, along with the dramatic asymmetry between upstream and downstream currents, observed experimentally can be attributed to the role bottom friction has in further retarding the advance of thinner currents.

Finally, the observable of primary interest is the storage efficiency E_s , shown for all five experiments in figure 11. Data points are shown using the symbols found in table 1 and are bounded by the numerical predictions for the largest and smallest values of the parameter governing fissure strength, $\bar{\lambda}$. We find that for all experiments in which $\bar{\lambda} \sim O(1)$, the drainage efficiency decreases to approximately 50% within a time less than $20 T$, as shown by the dashed line in figure 11.

5. Leakage from geological reservoirs

The propagation of buoyancy driven fluids within a porous medium has many applications within both industry and the environment. The societally important problem of CO₂ sequestration is of particular relevance to the present work. In typical carbon capture and storage schemes CO₂, a greenhouse gas, is first captured and then compressed and injected into subsurface reservoirs at depths typically greater than 1000 m where it behaves as a supercritical liquid. Since CO₂ is buoyant compared

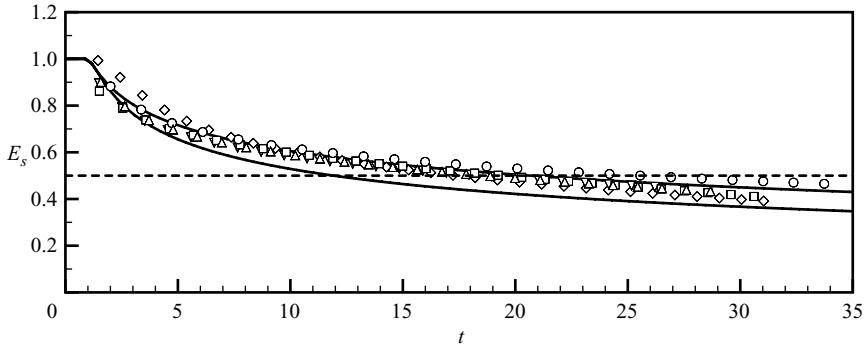


FIGURE 11. Efficiency of storage as defined by (3.21) for the five experiments detailed in table 1. Theoretical curves for the maximum ($\bar{\lambda}=0.626$, experiment 1) and minimum ($\bar{\lambda}=0.491$, experiment 1) values of the strength of the sink are compared to experimental measurements of the efficiency of storage for experiment 1 (\diamond), 2 (∇), 3 (\square), 4 (\circ) and 5 (\triangle). The horizontal dashed line indicates a storage efficiency of 50% which was reached in approximately $20 T \simeq 200$ s.

to the ambient brine it typically rises through the pore space and is trapped, especially at early times, by an impermeable seal at the top of the reservoir. Efforts to reduce significantly atmospheric levels of this greenhouse gas (and the concomitant climate change) rely on stable sequestration of CO_2 on time scales greater than 1000 years. In other words, the efficiency of storage must remain high over these time scales.

The largest industrial scale CO_2 sequestration project to date is the Sleipner project located in the North Sea. The Norwegian company Statoil has been removing CO_2 from a commercial natural gas stream and re-injecting the compressed CO_2 into the base of the Utsira formation since 1996. Seismic images taken over the course of injection have shown that the buoyant CO_2 rises and pools beneath a series of 9 thin shale layers spaced throughout the formation (Arts *et al.* 2004; Bickle *et al.* 2007). While these shale layers were never intended to act as long term barriers, they provide an ideal setting to test the ideas developed in this paper. Although it is clear from seismic images that fluid leaks through these relatively low permeability layers, it is unclear whether it does so in a relatively diffuse, spatially uniform, manner (Neufeld & Huppert 2009) or whether leakage is dominated by flow through a series of thin fissures. We shall assume the latter possibility and take $b \simeq 1.5$ m based on the seismically determined thickness of individual shale layers.

Our calculations directly address this issue when the typical height of the gravity current is much less than the thickness of the reservoir. A convenient means for estimating our model’s applicability is thus to compare the steady-state height at the injection point with the vertical extent of the reservoir.

Our model can be used to estimate the efficiency of storage in a saline aquifer possessing properties similar to those estimated for the Sleipner site. We consider a line of injection wells located a distance x_f from a fissure through an impermeable layer of thickness b . At Sleipner, Bickle *et al.* (2007) have made estimates of the average reservoir permeability, $k \approx 3.05 \times 10^{-12}$ m², the density and dynamic viscosity of injected CO_2 , $\rho_{\text{CO}_2} \approx 515$ kg m⁻³ and $\mu \approx 4 \times 10^{-5}$ Pa s, and the density of the ambient brine $\rho_{\text{brine}} \approx 1020$ kg m⁻³. Since it began operating in 1996 approximately 1 megatonne of CO_2 has been injected annually ($q \approx 0.062$ m² s⁻¹) into the reservoir where the inter-shale spacing is typically tens of metres. All of the parameters in our model are therefore reasonably well determined save for the fissure width W , and

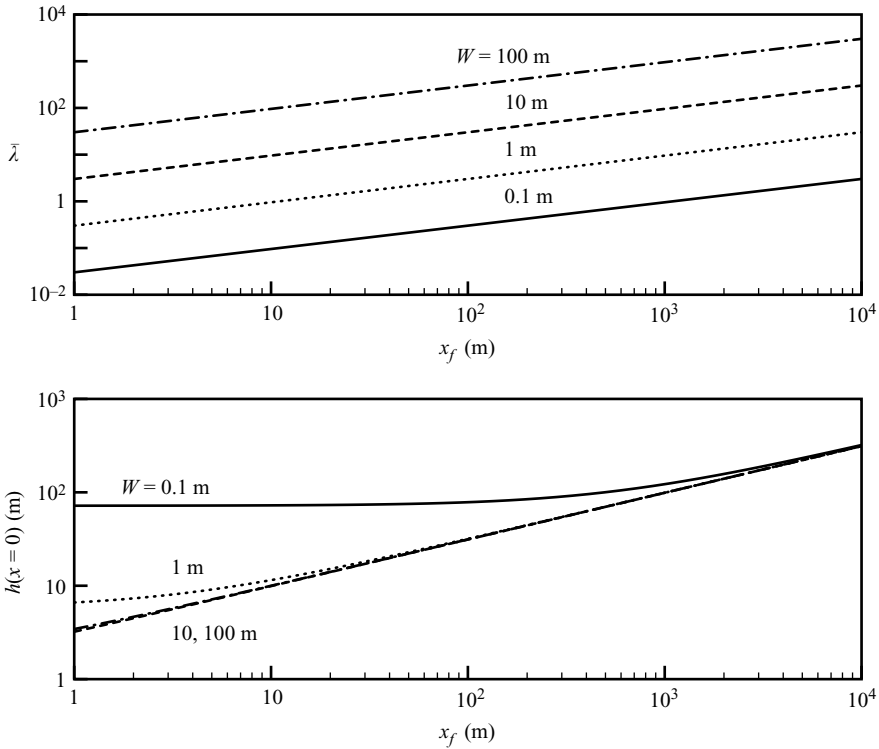


FIGURE 12. (a) Width-averaged strength of the fissure and (b) steady state height at the injection point shown in metres as functions of the distance from the fissure to the injection point in metres, for reservoir properties typical of the Sleipner site. In both cases, calculations are for a range of fissure widths: $W = 0.1$ m (solid), $W = 1$ m (dotted), $W = 10$ m (dashed) and $W = 100$ m (dash-dot).

position of the fissure x_f . Figure 12(a) shows the non-dimensional strength of the fissure $\bar{\lambda}$ as a function of the distance of the fissure from the injection point x_f for four differing fissure widths W . The corresponding steady-state height at the origin is shown in figure 12(b). Thus, we see that for fissures separated from the injection point by much greater than 100 m, flow within the aquifer becomes confined, and the model proposed in §2 is not applicable.

We can further assess the efficiency of storage for a representative fissure of width $W = 1$ m penetrating shale layers that are $b = 1.5$ m thick. In figure 13 the efficiency of storage is plotted as a function of time (in days) for a fissure of distance $x_f = 10, 100$ and 1000 m from the injection point. We see that inter-shale layer efficiency declines to 50% in $\tau = 13, 44$ and 458 days, respectively. The ultimate steady-state height at the injection point, where the current is thickest, for these representative parameter values is $h(0) = 12, 32$ and 99 m, respectively, indicating that for $x_f = 100$ and 1000 m our assumption of an unconfined reservoir may become invalid at late times.

In summary, we have shown that the model expressed by (2.7) can be used to assess the effectiveness of a reservoir for CO_2 sequestration. Using estimates for reservoir properties typical to the Sleipner site, we have shown that the efficiency of storage can decline dramatically in the presence of long fissures aligned parallel to the injection front. Furthermore, our analysis suggests that this decline in efficiency at each shale

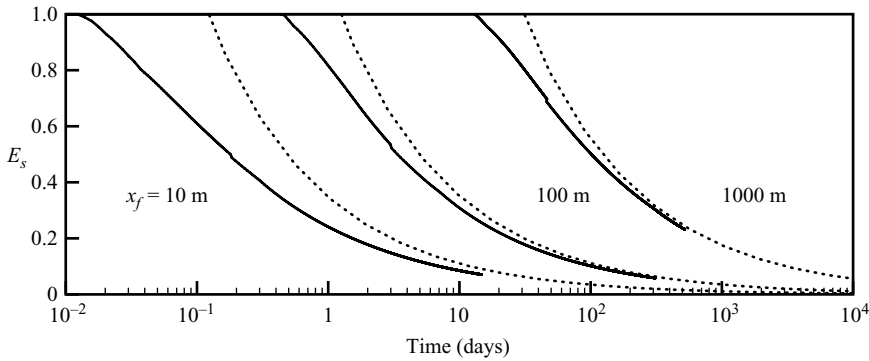


FIGURE 13. Efficiency of storage E_s as a function of time (in days) for fissures of permeability equal to the host reservoir and width $W = 1$ m for $x_f = 10, 100$ and 1000 m (left to right). The numerical solutions to (2.7) are plotted (solid) alongside the results of the asymptotic analysis (dotted). All parameters taken from Bickle *et al.* (2007) as discussed in the text.

layer happens over the course of, at most, 1 year, a prediction in keeping with the seismically observed vertical extent of CO_2 within the formation (Bickle *et al.* 2007).

6. Discussion and conclusion

We have assessed the spreading of a two-dimensional gravity current in a porous medium over an impermeable base punctuated by a single, discrete fissure located a distance x_f from the injection point. The model outlined in §2 allows both for drainage driven by the hydrostatic pressure above the fissure, and the weight of fluid within the fissure itself. The model presented here therefore differs from that of Pritchard (2007) in two important respects. First, the situation we consider is asymmetric about the input point rather than the symmetric case that Pritchard (2007) considered. Surprisingly, we find that even in the asymmetric case, where the current may propagate away from the fissure, the efficiency of storage is limited, and ultimately decreases as $t^{-1/2}$. Second, the law governing the leakage flux incorporates the driving force due to the weight of fluid filling the fissure. In our notation, Pritchard (2007) considered only the limit $\beta = 0$. We find that including the weight of fluid within the fissure itself only increases the rate of leakage, and can be asymptotically modelled by replacing $1/\bar{\lambda}$ with $1/\bar{\lambda} - \beta$.

By a combination of numerical and asymptotic investigations we have shown that the current ultimately reaches an asymmetric steady state, in which the flux at the injection point is exactly balanced by that leaking through the fissure. This is analogous to the situation found by Pritchard (2007). However, Pritchard (2007) did not study the efficiency of storage as defined by (3.21). Making use of (B7) from Pritchard (2007) we may calculate the efficiency of capture in the symmetric case, and find, in our notation,

$$E_{s,p} = 2 \frac{\phi'(1)}{\phi(1)^{1/2}} \bar{\lambda}^{-3/2} t^{-1/2}. \quad (t \gg 1) \tag{6.1}$$

We note, therefore, that in both symmetric and asymmetric two-dimensional geometries the efficiency of storage decays like $t^{-1/2}$ for $t \gg 1$. To compare our results with those of Pritchard (2007), it is convenient to consider the coefficient of $t^{-1/2}$ and so we introduce $e_s(\bar{\lambda}) \equiv E_s t^{1/2}$. An examination of (6.1) and (3.22) demonstrates

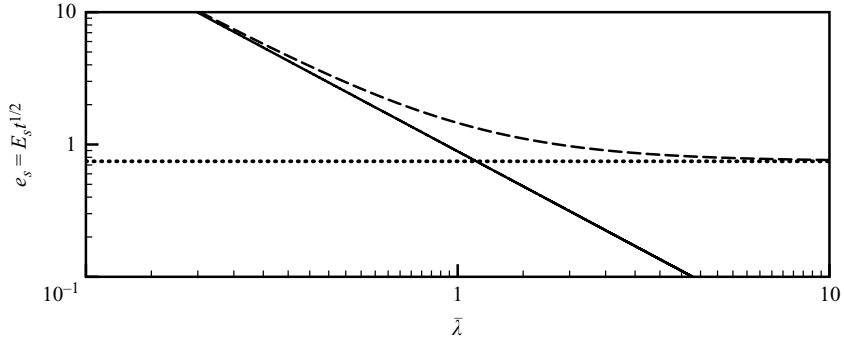


FIGURE 14. Dependence of efficiency of capture prefactor $e_s \equiv E_s t^{1/2}$ on the fissure parameter $\bar{\lambda}$ (here $\beta = 0$). Here the asymptotic results from both Pritchard's model, (6.1), (solid line) and the present model (3.22) (dashed curve) are plotted along with the limiting value $e_s \simeq 0.4437$ given by (3.22) in the limit $\bar{\lambda} \gg 1$ (dotted line).

that for large $\bar{\lambda}$, e_s is bounded below in the asymmetric geometry while it decreases indefinitely in the symmetric geometry considered by Pritchard (2007) as shown in figure 14. From this we conclude that in the limit of very strong fissures, the presence of asymmetry considerably increases the efficiency of storage. This leads on to the important question 'what happens for a point fissure in a three-dimensional situation?' This is a question we intend to address in the near future.

Experimental models of the system have confirmed both the initial evolution predicted by (2.7) and the form of the drainage law given by (2.1). Importantly, this provides experimental confirmation of the assumption, made both in this work and the work of Pritchard (2007), that leakage from a line fissure can be approximated by a jump in flux through a porous medium gravity current.

Finally, we note the relevance of such studies to the timely problem of CO₂ sequestration. The methodology presented in the present work provides a means both to assess the long-term efficacy of sequestration in a known reservoir and to address questions of uncertainty in the characterization of new reservoirs. These methods may prove critical in the regulation of industrial sequestration sites, where a detailed fully resolved numerical reservoir simulation encompassing all possible leakage routes may be computationally impractical. Such methods are therefore being brought to bear on the problems of radially spreading gravity currents in the presence of point fissures, as well as the two-dimensional and radial flow of CO₂ in confined aquifers. Finally, it is important to recognize that while the presence of an impermeable (or in this case semi-permeable) cap rock provides the principal means for geological sequestration on short to intermediate time scales, processes such as residual trapping, mixing of CO₂ with the host brine, and mineral formation may play an important role in the medium to longest time scales. The findings presented here therefore present the worst case scenario, an important first step in assessing the feasibility of long term geological storage as a means to combat anthropogenic climate change.

The authors would like to acknowledge the numerous helpful comments on many aspects of this work by John R. Lister and the experimental insight of Mark Hallworth. Valuable comments on an early draft of the manuscript were also provided by Peter Cook, Madeleine Golding, Charles Jenkins, Jan Nordbotten, Lincoln Paterson, David Pritchard and Daisuke Takagi. The research of D. Vella

is funded through a fellowship from the 1851 Royal Commission. J. A. Neufeld acknowledges support from a NERC grant and the research of H. E. Huppert is partially funded by a Royal Society Wolfson Research grant.

Appendix A. Numerical method

The nonlinear evolution equation describing the profile of the gravity current propagating past a fissure (2.7) was solved using a volume conservative, semi-implicit Crank–Nicholson scheme with adaptive time-stepping and adaptive grid size. Each time step was accomplished in two discrete iterations. In the first iteration the nonlinear terms in (2.7) were first estimated at the current time, and the profile was advanced forwards a full time step. During the second iteration, the nonlinear terms were estimated by the average of both current and future profiles. The drainage law given by (3.23) is implemented at a single grid cell centred at $x = 1$. For large $\bar{\lambda}$ and $h(1) \ll 1$ the drainage model given by (3.23) can result in a leakage flux through the fissure which exceeds that provided by the current to the grid cell at $x = 1$. We therefore require that the leakage flux through the grid cell located at $x = 1$ be the minimum of the flux input from the neighbouring grid cells and the leakage flux calculated by (3.23). Practically, this ensures that at each time step leakage through the fracture can at most reduce the height of the current above the fracture to $h \geq 0$.

Appendix B. The effect of bottom friction in a Hele-Shaw cell

To account for the effects of basal drag on the propagation of a gravity current in a Hele-Shaw cell, we assume that the profile of the current varies on a much larger spatial scale than either the dimensional plate spacing d or the dimensional current thickness h . In this limit, we may solve the Stokes equation for the horizontal velocity u , subject to the boundary conditions $u(z=0) = 0$ (no slip at the base) and $u_z(z=h) = 0$ (free slip at the free surface) by separation of variables as detailed in Happel & Brenner (1991). We find that

$$u = \frac{1}{2\mu} \frac{dp}{dx} y(y-d) + \sum_{m=1}^{\infty} A_m \sin \frac{m\pi y}{d} \cosh \frac{m\pi(z-h)}{d}, \quad (\text{B } 1)$$

where

$$A_m = -\frac{2d^2}{m^3\pi^3\mu} \frac{dp}{dx} \frac{\cos m\pi - 1}{\cosh m\pi h/d} \quad (\text{B } 2)$$

correcting a factor of 2 from Happel & Brenner (1991). The volume flux is given by

$$Q \equiv \int_0^h dz \int_0^d dy u = -\frac{d^3 h}{12\mu} \frac{dp}{dx} \left\{ 1 - \frac{96}{\pi^5} \frac{d}{h} \sum_{n=1}^{\infty} \frac{1}{(2n-1)^5} \tanh \left[\frac{(2n-1)\pi h}{d} \right] \right\}, \quad (\text{B } 3)$$

and the effective permeability of the Hele-Shaw cell is therefore

$$k_{eff} = \frac{d^2}{12} \left\{ 1 - \frac{96}{\pi^5} \frac{d}{h} \sum_{n=1}^{\infty} \frac{1}{(2n-1)^5} \tanh \left[\frac{(2n-1)\pi h}{d} \right] \right\} \quad (\text{B } 4)$$

as illustrated in figure 15. We observe that in the appropriate limits

$$k_{eff} \sim \frac{d^2}{12} \times \begin{cases} 1 - \frac{93}{\pi^5} \zeta(5) d/h, & d \ll h \\ 4h^2/d^2, & d \gg h \end{cases}, \quad (\text{B } 5)$$

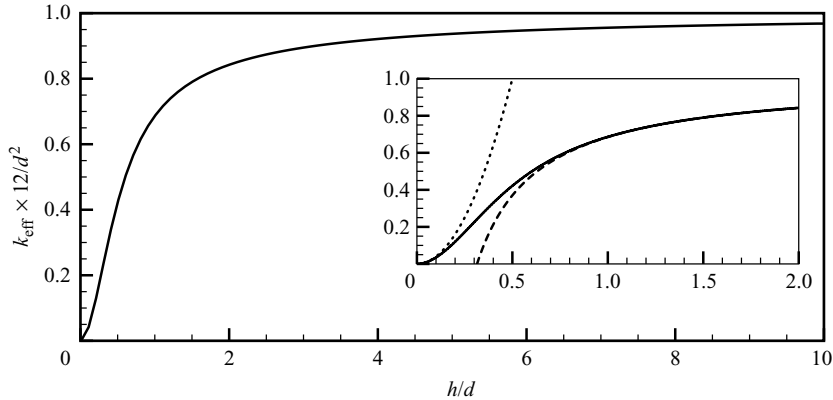


FIGURE 15. The dependence of the effective permeability of the Hele Shaw cell, k_{eff} , as a function of the height of the current measured relative to the width of the cell, h/d . Results from the computation of the infinite sum in (B4) (solid curve) are reproduced very well by the limiting forms found in (B5) (dashed curves). The inset shows the interval $[0, 2]$ over which the change between the asymptotic limits in (B5) occurs.

where $\zeta(5) \equiv \sum_{m=1}^{\infty} m^{-5} \approx 1.037$ is the Riemann zeta function of degree 5. This reproduces the standard permeability of a Hele-Shaw cell, $d^2/12$, for the case of currents that are very deep compared to d . In the limit $d \gg h$ we expect the current to behave as a viscous gravity current, a result consistent with an effective permeability $k_{\text{eff}} \sim h^2/3$. In all comparisons between the experimental results and numerical simulations the value of k_{eff} was computed correct to within 1% of its value as given by (B4).

REFERENCES

- ACTON, J. M., HUPPERT, H. E. & WORSTER, M. G. 2001 Two-dimensional viscous gravity currents flowing over a deep porous medium. *J. Fluid Mech.* **440**, 359–380.
- ANDERSON, D. M., McLAUGHLIN, R. M. & MILLER, C. T. 2003 The averaging of gravity currents in porous media. *Phys. Fluids* **15** (10), 2810–2829.
- ARTS, R., EIKEN, O., CHADWICK, A., ZWEIGEL, P., VAN DER MEER, L. & ZINSZNER, B. 2004 Monitoring of CO₂ injected at Sleipner using time-lapse seismic data. *Energy* **29**, 1383–1392.
- AVCI, C. B. 1994 Evaluation of flow leakage through abandoned wells and boreholes. *Water Resour. Res.* **30** (9), 2565–2578.
- BACHU, S. & BENNION, B. 2008 Effects of in-situ conditions on relative permeability characteristics of CO₂-brine systems. *Environ. Geol.* **54**, 1707–1722.
- BARENBLATT, G. I. 1996 *Scaling, Self-Similarity, and Intermediate Asymptotics*. Cambridge University Press.
- BEAR, J. 1972 *Dynamics of Fluids in Porous Media*. Dover.
- BICKLE, M., CHADWICK, A., HUPPERT, H. E., HALLWORTH, M. & LYLE, S. 2007 Modelling carbon dioxide accumulation at Sleipner: Implications for underground carbon storage. *Earth Planet. Sci. Lett.* **255**, 164–176.
- FARCAS, A. & WOODS, A. W. 2009 The effect of drainage on the capillary retention of CO₂ in a layered permeable rock. *J. Fluid Mech.* **618**, 349–359.
- HAPPEL, J. & BRENNER, H. 1991 *Low Reynolds Number Hydrodynamics: With Special Applications to Particulate Media*, 2nd edn. Kluwer Academic.
- HUPPERT, H. E. 2006 Gravity currents: a personal perspective. *J. Fluid Mech.* **554**, 299–322.

- HUPPERT, H. E. & WOODS, A. W. 1995 Gravity-driven flows in porous layers. *J. Fluid Mech.* **292**, 55–69.
- LYLE, S., HUPPERT, H. E., HALLWORTH, M., BICKLE, M. & CHADWICK, A. 2005 Axisymmetric gravity currents in a porous medium. *J. Fluid Mech.* **543**, 293–302.
- NEUFELD, J. A. & HUPPERT, H. E. 2009 Modelling carbon dioxide sequestration in layered strata. *J. Fluid Mech.* **625**, 353–370.
- NORDBOTTEN, J. M., CELIA, M. A. & BACHU, S. 2004 Analytical solutions for leakage rates through abandoned wells. *Water Resour. Res.* **40**, W04204, 1–10. doi:10.1029/2003WR002997.
- NORDBOTTEN, J. M., CELIA, M. A. & BACHU, S. 2005a Injection and storage of CO₂ in deep saline aquifers: analytical solution for CO₂ plume evolution during injection. *Trans. Porous Med.* **58**, 339–360.
- NORDBOTTEN, J. M., CELIA, M. A., BACHU, S. & DAHLE, H. 2005b Semi-analytical solution for CO₂ leakage through an abandoned well. *Environ. Sci. Technol.* **39**, 602–611.
- NORDBOTTEN, J. M., KAVETSKI, D., CELIA, M. A. & BACHU, S. 2009 Model for CO₂ leakage including multiple geological layers and multiple leaky wells. *Environ. Sci. Technol.* **43**, 743–749.
- PHILLIPS, O. M. 2009 *Geological Fluid Dynamics: Sub-Surface Flow and Reactions*. Cambridge University Press.
- PRITCHARD, D. 2007 Gravity currents over fractured substrates in a porous medium. *J. Fluid Mech.* **584**, 415–431.
- PRITCHARD, D. & HOGG, A. J. 2002 Draining viscous gravity currents in a vertical fracture. *J. Fluid Mech.* **459**, 207–216.
- PRITCHARD, D., WOODS, A. W. & HOGG, A. J. 2001 On the slow draining of a gravity current moving through a layered permeable medium. *J. Fluid Mech.* **444**, 23–47.
- SPANNUTH, M. J., NEUFELD, J. A., WETTLAUER, J. S. & WORSTER, M. G. 2009 Axisymmetric viscous gravity currents flowing over a porous medium. *J. Fluid Mech.* **622**, 135–144.
- VELLA, D. & HUPPERT, H. E. 2006 Gravity currents in a porous medium at an inclined plane. *J. Fluid Mech.* **555**, 353–362.
- WOODS, A. W. & FARCAS, A. 2009 Capillary entry pressure and the leakage of gravity currents through a sloping layered permeable rock. *J. Fluid Mech.* **618**, 361–379.